

Generalized Emergent Dark Energy: observational Hubble data constraints and stability analysis

A. Hernández-Almada^{1*}, Genly Leon^{2†}, Juan Magaña^{3‡},
Miguel A. García-Aspeitia^{4,5§}, V. Motta^{6¶}

¹ *Facultad de Ingeniería, Universidad Autónoma de Querétaro, Centro Universitario Cerro de las Campanas, 76010, Santiago de Querétaro, México*

² *Departamento de Matemáticas, Universidad Católica del Norte, Avda. Angamos 0610, Casilla 1280 Antofagasta, Chile*

³ *Instituto de Astrofísica & Centro de Astro-Ingeniería, Pontificia Universidad Católica de Chile, Av. Vicuña Mackenna, 4860, Santiago, Chile*

⁴ *Unidad Académica de Física, Universidad Autónoma de Zacatecas, Calzada Solidaridad esquina con Paseo a la Bufa S/N C.P. 98060, Zacatecas, México.*

⁵ *Consejo Nacional de Ciencia y Tecnología, Av. Insurgentes Sur 1582.*

Colonia Crédito Constructor, Del. Benito Juárez C.P. 03940, Ciudad de México, México.

⁶ *Instituto de Física y Astronomía, Universidad de Valparaíso, Avda. Gran Bretaña 1111, Valparaíso, Chile.*

Accepted YYYYMMDD. Received YYYYMMDD; in original form YYYYMMDD

ABSTRACT

Recently Li & Shafieloo (2019) proposed a phenomenologically emergent dark energy (PEDE) which consider that the dark energy density evolves as $\tilde{\Omega}_{\text{DE}}(z) = \Omega_{\text{DE},0} [1 - \tanh(\log_{10}(1+z))]$ with the advantage that it does not have degree of freedom. Later on, Li & Shafieloo (2020) proposed a generalized model by adding one degree of freedom to the PEDE model, encoded in the parameter Δ . Motivated by these proposals, we constrain the parameter space (h, Ω_m) and (h, Ω_m, Δ) for PEDE and Generalized Emergent Dark Energy (GEDE) respectively, by employing the most recent observational (non-) homogeneous Hubble data. Additionally, we reconstruct the deceleration and jerk parameters and estimate yield values at $z = 0$ of $q_0 = -0.784^{+0.028}_{-0.027}$ and $j_0 = 1.241^{+0.164}_{-0.149}$ for PEDE and $q_0 = -0.730^{+0.059}_{-0.067}$ and $j_0 = 1.293^{+0.194}_{-0.187}$ for GEDE using the homogeneous sample. We report values on the deceleration-acceleration transition redshift with those reported in the literature within 2σ CL. Furthermore, we perform a stability analysis of the PEDE and GEDE models to study the global evolution of the Universe around their critical points. Although the PEDE and GEDE dynamics are similar to the standard model, our stability analysis indicates that in both models there is an accelerated phase at early epochs of the Universe.

Key words: cosmology: theory, dark energy, cosmological parameters, observations.

1 INTRODUCTION

One of the most important challenges in modern cosmology is to elucidate the source of the accelerated expansion of the Universe, first evidenced by the high resolution observations of type Ia supernovae up to redshift $z \sim 1.2$ (Riess et al. 1998; Perlmutter et al. 1999) and then also confirmed by

the acoustic peaks (position) of the cosmic microwave background radiation measurements (Aghanim et al. 2018). In the framework of General Relativity (GR), the late cosmic acceleration is originated by an exotic component dubbed dark energy (DE). In the cosmological standard model, the nature of the dark energy is associated to the energy density of the vacuum (Λ), known as cosmological constant (Zel'dovich 1968; Weinberg 1989). One of the main properties of Λ is its equation of state, $w_\Lambda = -1$, implying an energy density constant over the cosmic time. The cosmological constant as DE has become a successful model to explain and fit several cosmological observations, however some theoretical aspects suggest that it might be necessary

* E-mail: ahalmada@uaq.mx

† E-mail: genly.leon@ucn.cl

‡ E-mail: jmagana@astro.puc.cl

§ E-mail: aspeitia@fisica.uaz.edu.mx

¶ E-mail: veronica.motta@uv.cl

to consider a dynamical dark energy. For instance, there is no convincing fundamental hypothesis to explain the cosmological constant dominates the dynamics of the universe at late times, this is commonly known as the coincidence problem. Another crucial difficulty is to reconcile the estimations of the Λ energy density from quantum field theory with those of the cosmological data. These problems have inspired plenty of models (see [Li et al. 2011](#), for a review) to explain that the late cosmic acceleration, some of them consider dynamical dark energy as a scalar field or a dark energy EoS parameterization ([Barboza & Alcaniz 2008](#); [Armendariz-Picon et al. 2001, 2000](#); [Linder 2003](#); [Chevallier & Polarski 2001](#); [Jassal et al. 2005](#); [Sendra & Lazkoz 2012](#); [Wetterich 1988](#); [Caldwell et al. 1998](#); [Caldwell 2002](#); [Chiba & Nakamura 1998](#); [Chiba et al. 2000](#); [Guo et al. 2005](#); [Magaña et al. 2017](#); [Román-Garza et al. 2019](#); [Amante et al. 2019](#)), interactions between dark energy and dark matter ([Caldera-Cabral et al. 2009](#); [Bolotin et al. 2015](#); [Di Valentino et al. 2019](#); [Hernández-Almada et al. 2020](#)), viscous DE ([Cruz et al. 2019](#); [Hernández-Almada 2019](#)), but also models without dark energy where the Einsteinian gravity is modified ([García-Aspeitia et al. 2018a, 2019c, 2018b, 2019b](#); [Övgün et al. 2018](#); [Hernández-Almada et al. 2019](#)), and more recently, models that propose an emergent DE whose energy density is $\rho_{DE}(z) \propto \tanh(z)$ ([Mortonson et al. 2009](#); [Dhawan et al. 2020](#); [Li & Shafieloo 2019, 2020](#)). Reviews on Dark Energy (theory and observations) can be found in ([Capozziello et al. 2006a,b](#); [Copeland et al. 2006](#); [Tsujikawa 2011](#); [Bamba et al. 2012](#); [Tsujikawa 2013](#), and references therein).

On the other hand, studies with observational data pointed out that the DE could be evolving as function of the scale factor or redshift ([Holsclaw et al. 2010](#); [Zhao et al. 2017](#); [Sola Peracaula et al. 2019](#)). Recently, the evidence from two different groups (Planck and Supernova Projects) show that there is a significant tension in the value of H_0 (between 4.0σ and 5.8σ), predicting, from Planck data a value of $H_0 = 67.4 \pm 0.5 \text{ km s}^{-1} \text{ Mpc}^{-1}$ ([Abbott et al. 2018](#)) with 1% of precision, while for Supernovae the value is $H_0 = 74. \pm 1.4 \text{ km s}^{-1} \text{ Mpc}^{-1}$ (see [Riess et al. \(2019\)](#), and [Verde et al. \(2019\)](#) for details). Another interesting unexplained phenomena is related to an excess of radiation detected by the Experiment to Detect the Global Epoch of Reionization (EDGES, [Bowman et al. \(2018\)](#)) at $z \sim 17$, which could be due to the interaction of dark matter with baryons but other explanations related to the presence of emergent DE in early epochs can not be discarded ([García-Aspeitia et al. 2019c,b](#)).

Therefore, it is plausible to consider, as a natural extension to the cosmological constant, dynamical dark energy (DDE) models as the cause for the accelerated expansion of the Universe. Recently, [Li & Shafieloo \(2019\)](#) introduced a phenomenological emergent dark energy model (PEDE), parameterizing the energy density of DE (with zero degree of freedom) using a hyperbolic tangent function, which is symmetric at logarithm scales (first attempts in the same line were done by [Mortonson et al. \(2009\)](#)). In this model, the DE is negligible at early times but at late times the contribution of Ω_{DE} increases, providing an alternative solution to the coincidence problem. The authors constrained the PEDE model using the latest data of Supernovae Ia (SNIa), Baryon Acoustic Oscillations (BAO) and the Planck measurements of Cosmic Microwave Background Radiation

(CMB) and claim that it can solve the known tension problem with the Hubble constant. In this vein, [Li & Shafieloo \(2020\)](#), generalized the PEDE model, constructing the Generalized Emergent Dark Energy model (GEDE), which contains two new parameters: Δ indicates the model we are dealing (PEDE or Λ CDM) and a transition redshift z_t , with $\Omega_{DE}(z_t) = \Omega_m(z_t)$, establishing a relationship between the matter density parameter and Δ (i.e. not a free parameter).

Here, we revisit and constrain the free parameters of the PEDE and GEDE models using the latest compilation of observational Hubble data (OHD). In addition, another vital study is the dynamical system analysis of these models. Dynamical systems analysis have provided to be very helpful to study the stability of several cosmological scenarios at background and perturbation levels ([Basilakos et al. 2019](#)), for instance, Teleparallel Dark Energy ([Xu et al. 2012](#); [Karpapoulos et al. 2018](#); [Cid et al. 2018](#)), Galileons ([Leon & Saridakis 2013](#); [De Arcia et al. 2016](#); [Giacomini et al. 2017](#); [Dimakis et al. 2017](#); [De Arcia et al. 2018](#)), Einstein-ether theories ([Latta et al. 2016](#); [Coley & Leon 2019](#); [Leon et al. 2020](#)), Hořava–Lifshitz theory ([Leon & Saridakis 2009](#); [Leon & Paliathanasis 2019](#)), Higher order Lagrangians ([Pulgar et al. 2015](#)), non-linear electrodynamics ([Övgün et al. 2018](#)), quintom models ([Lazkoz & Leon 2006](#); [Lazkoz et al. 2007](#); [Leon et al. 2018](#)), modified Jordan-Brans-Dicke theory ([Cid et al. 2016](#); [León et al. 2018](#); [Giacomini et al. 2020](#)), scalar field cosmologies ([Leon 2009](#); [Fadragas et al. 2014](#); [Fadragas & Leon 2014](#); [Leon & Silva 2019](#)), and other modified gravity models ([Leon et al. 2013](#); [Kofinas et al. 2014](#); [Leon & Saridakis 2015](#)). We investigate the stability of PEDE and GEDE models to search for different cosmic stages (i.e. radiation, matter, DE domination epochs) in order to demonstrate its feasibility with the standard Λ CDM model.

The paper is organized as follow: Sec. 2 we present the background cosmology of the PEDE and GEDE models. In Section 3, we constrain the parameters of PEDE and GEDE models using the latest sample of OHD, discussing the results in Sec. 3.1. Furthermore, in Sec. 4 we discuss the stability of both models through a dynamical system analysis. Finally, we present our remarks and conclusions in Sec. 5.

2 PHENOMENOLOGICAL EMERGENT DARK ENERGY COSMOLOGY

In this section we introduced the phenomenological emergent dark energy model proposed by [Li & Shafieloo \(2019\)](#) for which the DE is negligible at early times but it emerges at late times. We consider a flat Friedmann-Lemaître-Robertson-Walker (FLRW) metric which contains matter (m, dark matter plus baryons), radiation (r), and PEDE. The dynamics of this Universe is described by the Friedmann equation and the continuity equation for each component as:

$$H^2 \equiv \left(\frac{\dot{a}}{a}\right)^2 = \frac{8\pi G}{3}(\rho_{DE} + \rho_m + \rho_r), \quad (1a)$$

$$\dot{\rho}_{DE} + 3H(1 + w_{DE})\rho_{DE} = 0, \quad (1b)$$

$$\dot{\rho}_m + 3H(1 + w_m)\rho_m = 0, \quad (1c)$$

$$\dot{\rho}_r + 3H(1 + w_r)\rho_r = 0, \quad (1d)$$

where H is the Hubble parameter, a the scale factor, ρ_i is the energy density for each component, $w_{DE} = p_{DE}/\rho_{DE}$, $w_m =$

0, $w_r = 1/3$ are the equation of state for DE, matter and radiation respectively. By solving Eqs. (1b), (1c), (1d) we can rewrite the Eq. (1a) in terms of the density parameters, $\Omega = \rho_i/\rho_c$ ¹, and redshift, $z = 1/(1+a)$, as

$$H(z)^2 = H_0^2 \left[\Omega_m^{(0)} (1+z)^3 + \Omega_r^{(0)} (1+z)^4 + \tilde{\Omega}_{DE}(z) \right]. \quad (2)$$

The superscript (0) denotes quantities evaluated at $z = 0$ (or $a = 1$) and $\tilde{\Omega}_{DE}(z) = \Omega_{DE}^{(0)} f(z)$, where $\Omega_{DE}^{(0)} = 1 - \Omega_m^{(0)} - \Omega_r^{(0)}$ from the flatness condition:

$$\Omega_{DE} = 1 - \Omega_m - \Omega_r. \quad (3)$$

Notice that

$$f(z) \equiv \frac{\rho_{de}(z)}{\rho_{de}(0)} = \exp \left(3 \int_0^z \frac{1 + w_{DE}(z)}{1+z} dz \right). \quad (4)$$

Li & Shafieloo (2019) propose a phenomenological functional form for $f(z)$ and hence $\tilde{\Omega}_{DE}(z)$ as²

$$\tilde{\Omega}_{DE}(z) = \Omega_{DE}^{(0)} [1 - \tanh(\log_{10}(1+z))], \quad (5)$$

where $\tilde{\Omega}_{DE} \rightarrow 0$ at $z \rightarrow \infty$ and $\tilde{\Omega}_{DE} \rightarrow 1.4$ at $z \rightarrow -1$. Notice that

$$\begin{aligned} \Omega_{DE}(z) &= \frac{H_0^2}{H(z)^2} \tilde{\Omega}_{DE}(z) \\ &= \frac{H_0^2}{H(z)^2} \Omega_{DE}^{(0)} [1 - \tanh(\log_{10}(1+z))], \end{aligned} \quad (6)$$

Therefore, the dimensionless Friedmann equation results as

$$\begin{aligned} E(z) \equiv \frac{H(z)}{H_0} &= \left\{ \Omega_m^{(0)} (1+z)^3 + \Omega_r^{(0)} (1+z)^4 + \right. \\ &\left. \Omega_{DE}^{(0)} [1 - \tanh(\log_{10}(1+z))] \right\}^{1/2}, \end{aligned} \quad (7)$$

where the radiation density parameter at current epoch is calculated as $\Omega_r^{(0)} = 2.469 \times 10^{-5} h^{-2} (1 + 0.2271 N_{eff})$, with $N_{eff} = 3.04$ as the number of relativistic species (Komatsu & et. al. 2011), and h as the current Hubble dimensionless parameter. The PEDE EoS can be calculated as

$$w(z) = \frac{1}{3} \frac{d \ln \tilde{\Omega}_{DE}}{dz} (1+z) - 1. \quad (8)$$

By substituting (5) into Eq. (8) results

$$w(z) = -\frac{1}{3 \ln 10} (1 + \tanh[\log_{10}(1+z)]) - 1. \quad (9)$$

The deceleration parameter $q = -\ddot{a}a/\dot{a}^2$ can be rewritten in terms of redshift and $E(z)$ as:

$$\begin{aligned} q(z) &= \frac{(z+1)}{E(z)} \frac{dE(z)}{dz} - 1, \\ q(z) &= -1 + \frac{1}{2E(z)^2} \left[3\Omega_m^{(0)} (z+1)^3 + 4\Omega_r^{(0)} (z+1)^4 - \right. \\ &\quad \left. \Omega_{DE}^{(0)} \frac{\text{sech}^2 \left[\frac{\ln(z+1)}{\ln(10)} \right]}{\ln(10)} \right]. \end{aligned} \quad (10)$$

¹ The critical density is defined as $\rho_c \equiv 3H^2/8\pi G$.

² Where it is defined $\tilde{\Omega}_{DE}(z) \equiv \rho_{DE}/\rho_c^{(0)}$.

For completeness we also calculate the jerk parameter, $j \equiv \ddot{\ddot{a}}/a H^3$

$$\begin{aligned} j(z) &= q(z)^2 + \frac{(z+1)^2}{2E(z)^2} \frac{d^2 E(z)}{dz^2} - \frac{(z+1)^2}{4E(z)^4} \\ &\times \left(\frac{dE(z)}{dz} \right)^2, \end{aligned} \quad (11)$$

where

$$\begin{aligned} \frac{dE(z)}{dz} &= 3\Omega_m^{(0)} (1+z)^2 + 4\Omega_r^{(0)} (1+z)^3 - \\ &\Omega_{DE}^{(0)} \frac{\text{sech}^2 \left[\frac{\ln(z+1)}{\ln(10)} \right]}{(1+z) \ln(10)}, \\ \frac{d^2 E(z)}{dz^2} &= 6\Omega_m^{(0)} (1+z) + 12\Omega_r^{(0)} (1+z)^2 + \\ &\Omega_{DE}^{(0)} \frac{\text{sech}^2 \left[\frac{\ln(z+1)}{\ln(10)} \right]}{(1+z)^2 \ln(10)} + \Omega_{DE}^{(0)} \frac{2 \text{sech}^2 \left[\frac{\ln(z+1)}{\ln(10)} \right]}{(1+z)^2 \ln^2(10)} \times \\ &\tanh \left[\frac{\ln(z+1)}{\ln(10)} \right], \end{aligned} \quad (12)$$

which deviates from one, the jerk value for the cosmological constant.

2.1 Generalized emergent dark energy

Recently, Li & Shafieloo (2020) proposed a generalisation for the PEDE model also known as GEDE model by introducing

$$\tilde{\Omega}_{DE}(z) = \Omega_{DE}^{(0)} \frac{1 - \tanh \left(\Delta \log_{10} \left(\frac{1+z}{1+z_t} \right) \right)}{1 + \tanh \left(\Delta \log_{10} (1+z_t) \right)}, \quad (14)$$

where z_t is a transition redshift, $\Omega_{DE}(z_t) = \Omega_m^{(0)} (1+z_t)^3$, Δ is an appropriate dimensionless non-negative free parameter with the characteristic that if $\Delta = 0$ the Λ CDM model is recovered, and when $\Delta = 1$ and $z_t = 0$ the previously PEDE model is recovered. As z_t can be related to $\Omega_m^{(0)}$ and Δ , then z_t is not a free parameter. Notice that the DE density parameter is given by

$$\Omega_{DE} = \frac{H_0^2}{H^2} (1 - \Omega_m^{(0)} - \Omega_r^{(0)}) \frac{1 - \tanh \left(\Delta \log_{10} \left(\frac{1+z}{1+z_t} \right) \right)}{1 + \tanh \left(\Delta \log_{10} (1+z_t) \right)}. \quad (15)$$

The GEDE Friedmann equation is given by

$$\begin{aligned} E(z) \equiv \frac{H(z)}{H_0} &= \left[\Omega_m^{(0)} (1+z)^3 + \Omega_r^{(0)} (1+z)^4 + \right. \\ &\left. \Omega_{DE}^{(0)} \frac{1 - \tanh \left(\Delta \log_{10} \left(\frac{1+z}{1+z_t} \right) \right)}{1 + \tanh \left(\Delta \log_{10} (1+z_t) \right)} \right]^{1/2}. \end{aligned} \quad (16)$$

The EoS for GEDE model is given by

$$w(z) = -\frac{\Delta}{3 \ln 10} \left(1 + \tanh \left[\Delta \log_{10} \left(\frac{1+z}{1+z_t} \right) \right] \right) - 1. \quad (17)$$

The deceleration parameter reads

$$\begin{aligned} q(z) &= -1 + \frac{1}{2E(z)^2} \left[3\Omega_m^{(0)} (1+z)^3 + 4\Omega_r^{(0)} (1+z)^4 - \right. \\ &\quad \left. \Omega_{DE}^{(0)} \frac{\Delta}{\ln(10)} \frac{\text{sech}^2 \left[\frac{\Delta \ln \left(\frac{1+z}{1+z_t} \right)}{\ln(10)} \right]}{1 + \tanh \left(\Delta \log_{10} (1+z_t) \right)} \right]. \end{aligned} \quad (18)$$

As a complement, we also calculate the GEDE jerk parameter using Eq. (11), where

$$\frac{dE(z)^2}{dz} = 3\Omega_m^{(0)}(1+z)^2 + 4\Omega_r^{(0)}(1+z)^3 - \Omega_{DE}^{(0)} \frac{\Delta}{\ln(10)(1+z)} \frac{\text{sech}^2 \left[\frac{\Delta \ln \left(\frac{1+z}{1+z_t} \right)}{\ln(10)} \right]}{1 + \tanh(\Delta \log_{10}(1+z_t))}, \quad (19)$$

$$\frac{d^2 E(z)^2}{dz^2} = 6\Omega_m^{(0)}(1+z) + 12\Omega_r^{(0)}(1+z)^2 + \Omega_{DE}^{(0)} \frac{\Delta}{\ln(10)(1+z)^2} \frac{\text{sech}^2 \left[\frac{\Delta \ln \left(\frac{1+z}{1+z_t} \right)}{\ln(10)} \right]}{1 + \tanh(\Delta \log_{10}(1+z_t))} + \Omega_{DE}^{(0)} \frac{2\Delta^2}{\ln^2(10)(1+z)^2} \frac{\text{sech}^2 \left[\frac{\Delta \ln \left(\frac{1+z}{1+z_t} \right)}{\ln(10)} \right]}{1 + \tanh(\Delta \log_{10}(1+z_t))} \times \tanh \left[\frac{\Delta \ln \left(\frac{1+z}{1+z_t} \right)}{\ln(10)} \right]. \quad (20)$$

3 OBSERVATIONAL CONSTRAINTS

A canonical test is to confront a cosmological model with the observational Hubble data (OHD) which gives direct measurement of expansion rate of the Universe. Currently, the OHD sample is obtained from the differential age technique (Jimenez & Loeb 2002; Moresco et al. 2012) and BAO measurements. In this work, we consider the sample compiled by Magaña et al. (2018), which consists of 51 points in the redshift region $0.07 < z < 2.36$. It is worth to note that 31 data points come from the cosmic chronometers, i.e. passive galaxies, however, 20 data points of this sample are estimated from BAO measurements under different fiducial cosmologies (based on Λ CDM), which could provide biased constraints. Nevertheless, Magaña et al. (2018) present also homogeneous BAO OHD points calculated using the sound horizon at the drag epoch from Planck measurements. Here, we use the full sample with non-homogeneous and homogeneous OHD data points from BAO. Thus, the figure-of-merit is given by

$$\chi_{OHD}^2 = \sum_{i=1}^{51} \left(\frac{H_{th}(z_i, \Theta) - H_{obs}(z_i)}{\sigma_{obs}^i} \right)^2, \quad (21)$$

where $H_{th}(z_i, \Theta) - H_{obs}(z_i)$ denotes the difference between the theoretical Hubble parameter with parameter space $\Theta = (h, \Omega_{dm}^{(0)})$ and $(h, \Omega_{dm}^{(0)}, \Delta)$ for PEDE and GEDE models respectively, and the observational one at the redshift z_i , and σ_{obs}^i is the uncertainty of H_{obs}^i .

To constrain the PEDE and GEDE cosmological parameters we perform a Markov chain Monte Carlo (MCMC) analysis employing the emcee Python module (Foreman-Mackey et al. 2013). We consider Gaussian likelihoods $\mathcal{L} \propto e^{-\chi^2/2}$, a Gaussian prior over h centered at $h = 0.7403 \pm 0.0142$ (Riess et al. 2019, R19, hereafter) and a flat prior over $\Omega_m^{(0)} : [0, 1]$ for both, PEDE and GEDE models. Additionally, we consider a flat prior on $\Delta : [0, 10]$. Notice that the parameter z_t presented in the GEDE model is related to the parameter Δ through the condition $\Omega_{DE}(z_t) = \Omega_m(z_t)$.

As a complement, we perform a similar analysis but alternatively using a flat prior on $h : [0, 1]$. Our analysis consider a burn-in phase which is stopped when the Gelman-Rubin convergence criteria (< 1.1) is fulfilled and a MCMC phase with 3000 steps and 500 walkers for each one.

3.1 Results

In this section we report our results obtained in Bayesian analysis. In Table 1 are provided the mean values for the parameters and their uncertainties estimated at 1σ in both scenarios and using the homogeneous and non-homogeneous OHD. Additionally, we also report the parameter mean values when a flat prior over h is considered. These are in agreement with those obtained using a Gaussian prior on h . Our constraints are very similar to those obtained by Li & Shafieloo (2019), estimating a deviation on Δ within 1σ CL with the one estimated by Li & Shafieloo (2019) from a CMB+ h (R19) joint analysis. Figure 1 shows the 2D confidence region at 68% (1σ), 95% (2σ) and 99.7% (3σ) of the free parameters for GEDE (top panel) and PEDE (bottom panel) models, using the homogeneous and non-homogeneous OHD, respectively. Additionally, their 1D posterior distributions are presented. It is worth to note that although the homogeneous sample provides slightly broader confidence contours than those obtained with the non-homogeneous sample, the constraints are less (cosmology-model) unbiased. As it is expected, we find an anti-correlation relation between $\Omega_m^{(0)}$ and h for both models. For GEDE model, we also observe a positive correlation between Δ and h . For the GEDE model, our Δ constraints are in tension with $\Delta = 1.13 \pm 0.28$ obtained by Li & Shafieloo (2020) employing CMB and the H_0 measurements. Figure 2 shows the comparison of the Hubble parameter in GEDE and PEDE cosmologies with the observational ones including non-homogeneous and homogeneous BAO OHD points. Notice that both models provide a good fit to the data.

Figure 3 shows the reconstruction of the deceleration parameter as a function of redshift for both, PEDE and GEDE models when the non homogeneous and homogeneous OHD are employed. The universe undergoes a transition from decelerated to accelerated expansion at redshift $0.784_{-0.044}^{+0.044}$ and $0.809_{-0.057}^{+0.057}$ for the PEDE and GEDE models respectively (homogeneous OHD). Our constraints are consistent at 1.95σ and 1.1σ respectively with the results by Jesus et al. (2018). Additionally, the reconstruction of the jerk parameter for both models is shown in Figure 4. By construction the PEDE and GEDE are DDE models, hence the jerk evolves as a function of the scale factor and it is not equal to one as in the cosmological constant paradigm. We also report the deceleration and jerk parameters at $z = 0$, q_0 and j_0 , we estimate yield values of $q_0 = -0.784_{-0.027}^{+0.028}$, $-0.784_{-0.027}^{+0.028}$ and $j_0 = 1.241_{-0.149}^{+0.164}$, $1.487_{-0.011}^{+0.010}$ for PEDE using homogeneous and non-homogeneous OHD, respectively. Similarly, we estimate $q_0 = -0.730_{-0.067}^{+0.059}$, $-0.715_{-0.058}^{+0.050}$ and $j_0 = 1.293_{-0.187}^{+0.194}$, $1.241_{-0.149}^{+0.164}$ for GEDE when homogeneous and non-homogeneous OHD are considered.

Table 1. Mean values of the free parameters for GEDE and PEDE models using homogeneous and non-homogeneous OHD and a Gaussian prior on $h = 0.7403 \pm 0.0142$ (Riess et al. 2019). The last column is the redshift z_t with $\Omega_m(z_t) = \Omega_{DE}(z_t)$. The uncertainties reported correspond to 1σ confidence level. In parenthesis are the best fit values when a flat prior on h is considered in the region $[0, 1]$.

Sample	χ^2	h	$\Omega_m^{(0)}$	Δ	z_t
PEDE					
homogeneous OHD	24.5 (24.5)	$0.740^{+0.011}_{-0.011}$ ($0.738^{+0.018}_{-0.018}$)	$0.252^{+0.016}_{-0.015}$ ($0.254^{+0.024}_{-0.022}$)	1.0	0
non-homogeneous OHD	32.1 (32.1)	$0.740^{+0.010}_{-0.010}$ ($0.740^{+0.014}_{-0.014}$)	$0.249^{+0.013}_{-0.013}$ ($0.249^{+0.018}_{-0.016}$)	1.0	0
GEDE					
homogeneous OHD	23.7 (23.0)	$0.735^{+0.012}_{-0.012}$ ($0.725^{+0.023}_{-0.020}$)	$0.247^{+0.018}_{-0.017}$ ($0.256^{+0.025}_{-0.022}$)	$0.690^{+0.624}_{-0.457}$ ($0.533^{+0.712}_{-0.390}$)	$0.403^{+0.058}_{-0.057}$ ($0.385^{+0.058}_{-0.056}$)
non-homogeneous OHD	30.2 (28.6)	$0.731^{+0.012}_{-0.011}$ ($0.718^{+0.017}_{-0.015}$)	$0.245^{+0.014}_{-0.013}$ ($0.255^{+0.018}_{-0.017}$)	$0.539^{+0.470}_{-0.352}$ ($0.332^{+0.472}_{-0.244}$)	$0.417^{+0.044}_{-0.043}$ ($0.403^{+0.043}_{-0.043}$)

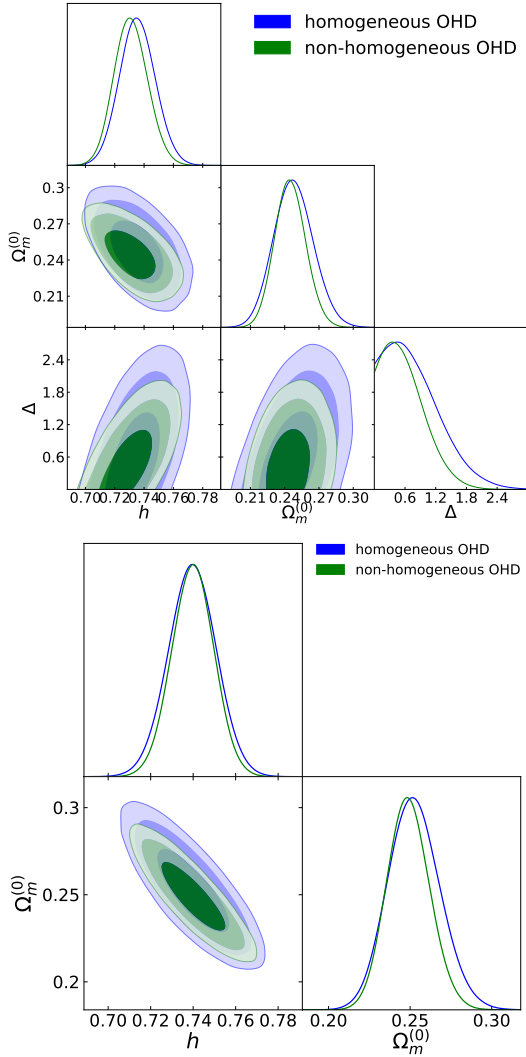


Figure 1. 1D posterior distributions and 2D contours of the free parameters for GEDE (top panel) and PEDE (bottom panel) models at 1σ , 2σ , 3σ CL (from darker to lighter respectively). The blue (green) contours correspond to the space constrained using (non-) homogeneous OHD.

4 DYNAMICAL SYSTEM ANALYSIS

In this section, we investigate the PEDE and GEDE models from the dynamical system approach to obtain the critical points and stability conditions of the models. This phase-space and stability examination let us to bypass the non-

linearities of the cosmological equations, and facilitates a complete analytical treatment, to obtain a qualitative description of the global dynamics of these scenarios, which is independent of the initial conditions and the specific evolution of the universe. Furthermore, in these asymptotic solutions we are able to calculate various observable quantities, such as the DE and total equation-of-state parameters, the deceleration parameter, the density parameters for the different species, etc., that allows us to classify the solution.

In order to perform the stability analysis of a given cosmological scenario, one first transforms it to its autonomous form $\mathbf{X}' = \mathbf{f}(\mathbf{X})$ (Wainwright & Ellis 1997; Ferreira & Joyce 1997; Copeland et al. 1998; Perko 2000; Coley 2003; Copeland et al. 2006; Chen et al. 2009; Cotsakis & Kittou 2013; Giambo & Miritzis 2010), where \mathbf{X} is a column vector containing some auxiliary variables and primes denote derivative with respect to a time variable (conveniently chosen). Then, one extracts the critical points \mathbf{X}_c by imposing the condition $\mathbf{X}' = \mathbf{0}$, and in order to determine their stability properties, one expands around them with \mathbf{U} the column vector of the perturbations of the variables. Therefore, for each critical point the perturbation equations are expanded to first order as $\mathbf{U}' = \mathbf{Q} \cdot \mathbf{U}$, with the matrix \mathbf{Q} containing the coefficients of the perturbation equations. The eigenvalues of \mathbf{Q} determine the type and stability of the specific critical point.

4.1 PEDE model

To start our analysis, it is convenient to write the cosmic evolution equations in terms of the scale factor. Using the rule

$$\frac{d\rho_i}{dt} = \frac{d\rho_i}{da} \frac{da}{dt} = aH \frac{d\rho_i}{da}, \quad (22)$$

and using units where $8\pi G = 1$, the field equations are written as

$$\rho'_{DE}(a) + 3(1 + w(a)) \frac{\rho_{DE}(a)}{a} = 0, \quad (23a)$$

$$\rho'_m(a) + 3 \frac{\rho_m(a)}{a} = 0, \quad (23b)$$

$$\rho'_r(a) + 4 \frac{\rho_r(a)}{a} = 0, \quad (23c)$$

$$\frac{H'(a)}{H(a)} = -\frac{3}{2}(1 + w(a)) \frac{\Omega_{DE}}{a} - \frac{3}{2} \frac{\Omega_m}{a} - 2 \frac{\Omega_r}{a}, \quad (23d)$$

$$3H^2(a) = \rho_{DE}(a) + \rho_m(a) + \rho_r(a). \quad (23e)$$

Integrating (23a) with the EoS $w(a)$ given by

$$w(a) = -\frac{1}{3 \ln 10} (1 - \tanh[\log_{10} a]) - 1, \quad (24)$$

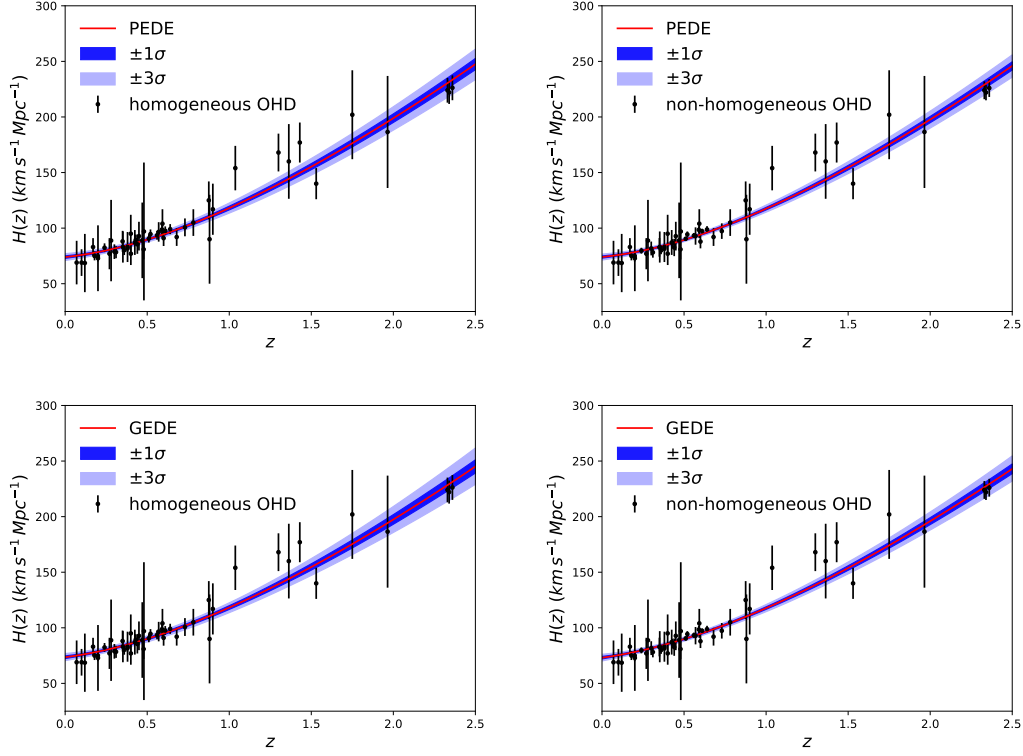


Figure 2. Best fits over (non-)homogeneous OHD sample at left side (right side) of the panel for PEDE (top panel) and GEDE (bottom panel). The darker (lighter) band represents the uncertainty at 1σ (3σ) CL.

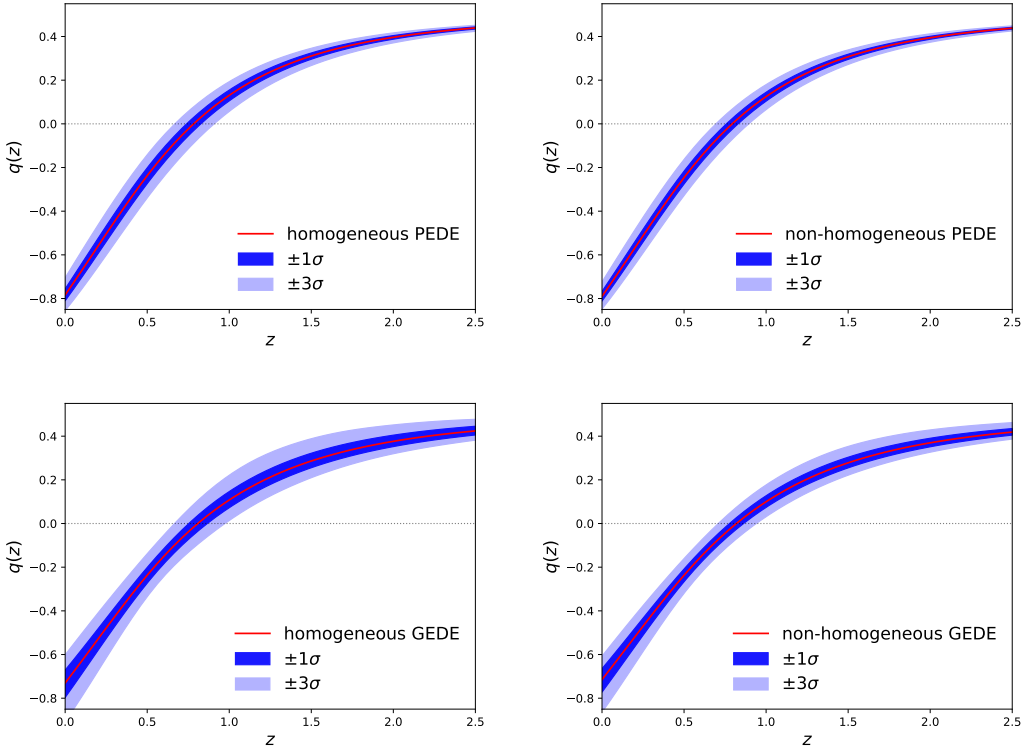


Figure 3. Reconstruction of the deceleration parameter for PEDE (top panel) and GEDE (bottom panel) respectively. The darker (lighter) band represents the uncertainty at 1σ (3σ) CL.

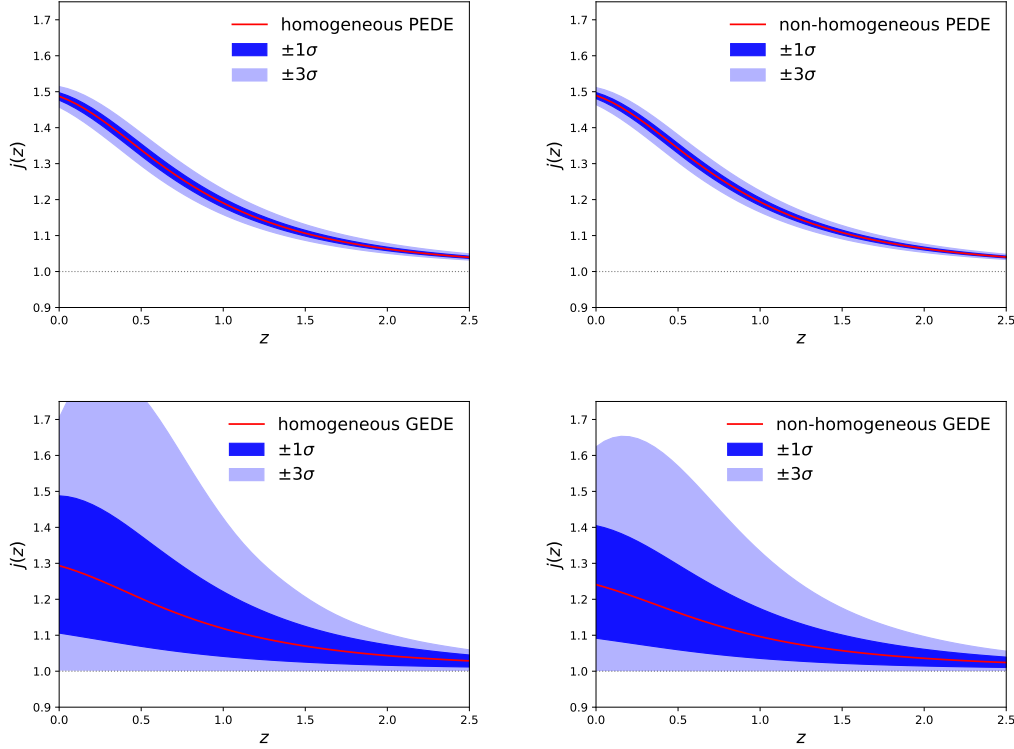


Figure 4. Reconstruction of the jerk parameter for PEDE (top panel) and GEDE (bottom panel). The darker (lighter) band represents the uncertainty at 1σ (3σ) CL.

and considering $\rho_{DE}^{(0)} = \rho_{DE}|_{a=1} = 3H_0^2\Omega_{DE}^{(0)}$ we obtain

$$\rho_{DE}(a) = 3H_0^2\Omega_{DE}^{(0)} (\tanh(\log_{10}(a)) + 1). \quad (25)$$

Hence,

$$\Omega_{DE} = \frac{H_0^2}{H^2} (1 - \Omega_m^{(0)} - \Omega_r^{(0)}) [1 + \tanh(\log_{10}a)]. \quad (26)$$

Defining the time variable $\tau = \log_{10} a$, we have $\frac{df}{d\tau} = \ln(10)a \frac{df}{da}$. Alternatively, we can define the time derivative $\frac{df}{d\bar{\tau}} = \frac{H_0^2}{(H_0+H)^2} \frac{df}{d\tau}$. The new time variable $\bar{\tau}$ can be calculated as a function of the redshift through

$$\begin{aligned} \frac{d\bar{\tau}}{dz} &= -\frac{(1+E(z))^2}{(1+z)\ln 10} \\ &= -\frac{1}{(1+z)\ln 10} \left(1 + \left[\Omega_m^{(0)}(1+z)^3 + \Omega_r^{(0)}(1+z)^4 \right. \right. \\ &\quad \left. \left. + \Omega_{DE}^{(0)} [1 - \tanh(\log_{10}(1+z))] \right]^{1/2} \right)^2. \end{aligned} \quad (27)$$

Defining

$$T = \frac{H_0}{H_0+H}, \quad \Omega_m = \frac{H_0^2\Omega_m^{(0)}}{a^3H^2}, \quad \Omega_r = \frac{H_0^2\Omega_r^{(0)}}{a^4H^2}, \quad (28)$$

$E(z)$ is related to $T(z)$ by

$$E(z) = \frac{H}{H_0} = \frac{1-T}{T}. \quad (29)$$

Therefore,

$$\Omega_{DE} = \frac{T^2}{(1-T)^2} (1 - \Omega_m^{(0)} - \Omega_r^{(0)}) [1 + \tanh(\log_{10}a)]. \quad (30)$$

On the other hand, due to the flatness condition (3) we obtain the restriction

$$\frac{1 - \Omega_m - \Omega_r}{(1 - \Omega_m^{(0)} - \Omega_r^{(0)})} = \frac{T^2}{(1-T)^2} [1 + \tanh(\log_{10}a)]. \quad (31)$$

This implies that the equation of state can be expressed as a function of the phase space variables, that is,

$$w(T, \Omega_m, \Omega_r) = -1 - \frac{1}{3\ln 10} \left[2 - \frac{(1 - \Omega_m - \Omega_r)(1-T)^2}{(1 - \Omega_m^{(0)} - \Omega_r^{(0)})T^2} \right]. \quad (32)$$

The dynamical system for the vector state $(T, \Omega_m, \Omega_r)^T$ is now given by

$$\begin{aligned} \frac{dT}{d\bar{\tau}} &= \frac{1}{2} (1-T) T^3 (2(\Omega_m + \Omega_r - 1) + \ln(10)(3\Omega_m + 4\Omega_r)) \\ &\quad + \frac{(1-T)^3 T (1 - \Omega_m - \Omega_r)^2}{2(1 - \Omega_m^{(0)} - \Omega_r^{(0)})}, \end{aligned} \quad (33a)$$

$$\begin{aligned} \frac{d\Omega_m}{d\bar{\tau}} &= T^2 \Omega_m (\ln(10)(3\Omega_m + 4\Omega_r - 3) + 2(\Omega_m + \Omega_r - 1)) \\ &\quad + \frac{(1-T)^2 \Omega_m (1 - \Omega_m - \Omega_r)^2}{(1 - \Omega_m^{(0)} - \Omega_r^{(0)})}, \end{aligned} \quad (33b)$$

$$\begin{aligned} \frac{d\Omega_r}{d\bar{\tau}} &= T^2 \Omega_r (\Omega_m (2 + 3\ln(10)) + 2(\Omega_r - 1)(1 + 2\ln(10))) \\ &\quad + \frac{(1-T)^2 \Omega_r (1 - \Omega_m - \Omega_r)^2}{(1 - \Omega_m^{(0)} - \Omega_r^{(0)})}, \end{aligned} \quad (33c)$$

defined on the bounded phase space $\{(T, \Omega_m, \Omega_r) \in \mathbb{R}^3 : 0 \leq T \leq 1, \Omega_m + \Omega_r \leq 1, \Omega_m \geq 0, \Omega_r \geq 0\}$. We have three parameters in the model, $\Omega_m^{(0)}, \Omega_r^{(0)}, \Omega_{DE}^{(0)} = 1 - \Omega_m^{(0)} - \Omega_r^{(0)}$, which represent the values of $\Omega_m, \Omega_r, \Omega_{DE}$ at redshift $z = 0$ ($T = 0.5$). For the PEDE model, these param-

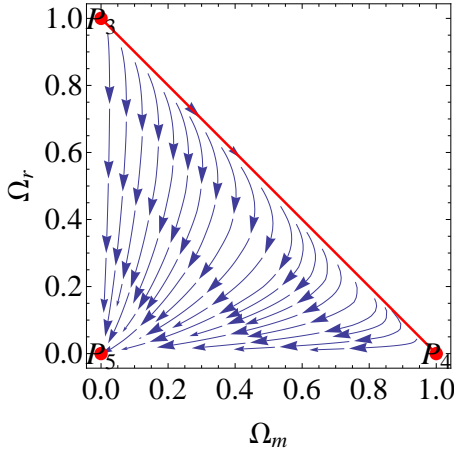


Figure 5. Dynamics of the system (33) on the invariant set $T = 1$. The equilibrium point $P_3 : (1, 0, 1)$ is a local source, $P_4 : (1, 1, 0)$ is a saddle and $P_5 : (1, 0, 0)$ is a local sink (but a saddle in the 3D phase space).

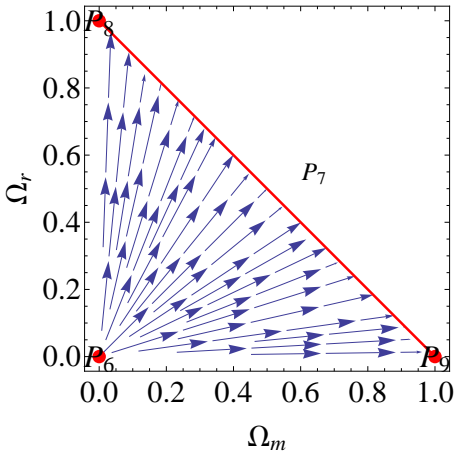


Figure 6. Dynamics of the system (33) on the invariant set $T = 0$. The line $P_7 : (0, \Omega_m, 1 - \Omega_m)$, and its endpoints P_8 and P_9 are local attractors. P_6 is the global source.

eters are constrained in previous section, for the following qualitative and numerical analysis we take the homogeneous constraints, $(\Omega_m^{(0)}, \Omega_r^{(0)}, \Omega_{DE}^{(0)}) = (0.252, 7.62 \times 10^{-5}, 0.747)$, which are less unbiased for any fiducial cosmological model (see §3). Notice that multiplying term by term the system (33) by the equation (27), results in a system which can be integrated in terms of redshift.

We can study the dynamical system (33) as we discussed in Table 2. The system (33) admits two relevant invariant sets $T = 1$ and $T = 0$. The variable T satisfies $T \rightarrow 0$ when $H \rightarrow \infty$; $T \rightarrow 1$ when $H \rightarrow 0$; and $T = 0.5$ when $H \rightarrow H_0$. In the invariant set $T = 1$ the dynamics of the system (33) is as shown in Fig. 5. The equilibrium point $P_3 : (1, 0, 1)$ is a local source, $P_4 : (1, 1, 0)$ is a saddle and $P_5 : (1, 0, 0)$ is a local sink (but a saddle in the 3D phase space). On the other hand, the dynamics at the invariant set $T = 0$ is governed by an integrable 2D dynamical system such that the orbit passing through $(T, \Omega_m, \Omega_r) = (0, \Omega_{m,0}, \Omega_{r,0})$ at $\bar{\tau} = \bar{\tau}_0$ is

given by

$$\Omega_r(\Omega_m) = \frac{\Omega_m \Omega_{r,0}}{\Omega_{m,0}}. \quad (34)$$

For this solution, the relation between $\bar{\tau}$ and Ω_m is

$$\begin{aligned} \bar{\tau}(\Omega_m) = \bar{\tau}_0 + & \frac{(\Omega_m - \Omega_{m,0})(1 - \Omega_m^{(0)} - \Omega_r^{(0)})(1 - \Omega_{m,0} - \Omega_{r,0})}{(\Omega_{m,0} - \Omega_{r,0})((1 - \Omega_m)\Omega_{m,0} - \Omega_m\Omega_{r,0})} \\ & + (1 - \Omega_m^{(0)} - \Omega_r^{(0)}) \ln \left(\frac{\Omega_m(1 - \Omega_{m,0} - \Omega_{r,0})}{(1 - \Omega_m)\Omega_{m,0} - \Omega_m\Omega_{r,0}} \right). \end{aligned} \quad (35)$$

Figure 6 illustrates the dynamics of the system (33) on the invariant set $T = 0$. The line $P_7 : (0, \Omega_m, 1 - \Omega_m)$, and the endpoints P_8 and P_9 are local attractors. P_6 is the source ($\bar{\tau}$ was re scaled by the factor $1 - \Omega_m^{(0)} - \Omega_r^{(0)} > 0$).

In the 3D phase space, the late-time attractors are the equilibrium points $P_{1,2}$ with $T = \frac{1}{1 \pm \sqrt{2\Omega_{DE}^{(0)}}}$, $\Omega_m = 0$, $\Omega_r = 0$.

Therefore $H_{\pm} = \pm \sqrt{2\Omega_{DE}^{(0)}} H_0$. The corresponding cosmological solutions are $a_{\pm}(t) = a_0 e^{\pm \sqrt{2\Omega_{DE}^{(0)}} H_0 t}$. The choice $+$, that corresponds to P_1 , belongs to an ever expanding de Sitter solution. The solution corresponding to P_2 satisfies $a \rightarrow 0$ at late times; an static solution. However, this solution is not physical because the condition $T \geq 0$ requires $0 \leq \Omega_{DE}^{(0)} < \frac{1}{2}$, which is not supported (at $> 5\sigma$) neither by the narrow bound placed by Planck data $\Omega_{DE}^{(0)} = 0.6889 \pm 0.0056$ (Abbott et al. 2018), nor by our value $\Omega_{DE}^{(0)} = 0.748_{-0.015}^{+0.016}$. There are three solutions P_3 , P_4 and P_5 dominated by radiation, DM and DE, respectively, that satisfy $T = 1$. This means that $H = 0$ for these solutions, and they are saddles. The point P_6 is the source, it satisfies $\Omega_m = 0$, $\Omega_r = 0$, therefore, it is dominated by DE. As $T = 0$, this implies that $H \rightarrow \infty$. Because it is a source, it represents the initial stages of the cosmic evolution, dominated by DE. This means that for the model not only dark energy accounts for the recent accelerated phase of the evolution but also the initial stage is driven by an accelerated dark-energy dominated expanding phase.

To analyse the nonhyperbolic points P_7 , P_8 and P_9 that satisfy $T \rightarrow 0$, we rely on numerical examination, where we see that they behave as saddles as shown in the top of Fig. 7. However, when the dynamics is restricted to the invariant set $T = 0$, it is governed by an integrable 2D dynamical system, such that the line $P_7 : (0, \Omega_m, 1 - \Omega_m)$, along with the endpoints P_8 and P_9 , are local attractors (as shown in Fig. 6), whereas P_6 is the global source.

4.2 GEDE model

In this section we investigate the GEDE model with Ω_{DE} given by Eq. (15) whose evolution is given by (1) with $w(z)$ defined by (17).

Due to the flatness condition given by Eq. (3) we obtain the restriction

$$\frac{1 - \Omega_m - \Omega_r}{(1 - \Omega_m^{(0)} - \Omega_r^{(0)})} = \frac{T^2}{(1 - T)^2} \left[\frac{1 - \tanh \left(\Delta \log_{10} \left(\frac{1+z}{1+z_t} \right) \right)}{1 + \tanh \left(\Delta \log_{10} (1 + z_t) \right)} \right]. \quad (36)$$

Table 2. Stability of the equilibrium points of the system (33).

Label	(T, Ω_m, Ω_r)	Eigenvalues	Stability
P_1	$\left(\frac{1}{1+\sqrt{2\Omega_{DE}^{(0)}}}, 0, 0\right)$	$\left\{-\frac{2}{\left(\sqrt{2\Omega_{DE}^{(0)}}+1\right)^2}, -\frac{3\ln(10)}{\left(\sqrt{2\Omega_{DE}^{(0)}}+1\right)^2}, -\frac{4\ln(10)}{\left(\sqrt{2\Omega_{DE}^{(0)}}+1\right)^2}\right\}$	sink
P_2	$\left(\frac{1}{1-\sqrt{2\Omega_{DE}^{(0)}}}, 0, 0\right)$	$\left\{-\frac{2}{\left(\sqrt{2\Omega_{DE}^{(0)}}-1\right)^2}, -\frac{3\ln(10)}{\left(\sqrt{2\Omega_{DE}^{(0)}}-1\right)^2}, -\frac{4\ln(10)}{\left(\sqrt{2\Omega_{DE}^{(0)}}-1\right)^2}\right\}$	sink
P_3	$(1, 0, 1)$	$\{2+4\ln(10), -2\ln(10), \ln(10)\}$	saddle
P_4	$(1, 1, 0)$	$\left\{2+3\ln(10), -\frac{3\ln(10)}{2}, -\ln(10)\right\}$	saddle
P_5	$(1, 0, 0)$	$\{-2(1+2\ln(10)), -2-3\ln(10), 1\}$	saddle
P_6	$(0, 0, 0)$	$\left\{\frac{1}{1-\Omega_m^{(0)}-\Omega_r^{(0)}}, \frac{1}{1-\Omega_m^{(0)}-\Omega_r^{(0)}}, \frac{1}{2(1-\Omega_m^{(0)}-\Omega_r^{(0)})}\right\}$	source
P_7	$(0, \Omega_m, 1-\Omega_m)$	$\{0, 0, 0\}$	nonhyperbolic
P_8	$(0, 0, 1)$	$\{0, 0, 0\}$	nonhyperbolic
P_9	$(0, 1, 0)$	$\{0, 0, 0\}$	nonhyperbolic

This implies that the equation of state can be expressed as a function of the phase space variables, that is,

$$w(T, \Omega_m, \Omega_r) = \Delta \left(2 - \frac{(T-1)^2(\Omega_m + \Omega_r - 1) \left(\tanh\left(\frac{\Delta \ln(z_t + 1)}{\ln(10)}\right) + 1 \right)}{T^2(\Omega_m^{(0)} + \Omega_r^{(0)} - 1)} \right) - 1 - \frac{3\ln(10)}{3\ln(10)}. \quad (37)$$

In this case we calculate $\bar{\tau}$ as a function of the redshift through

$$\begin{aligned} \frac{d\bar{\tau}}{dz} &= -\frac{(1+E(z))^2}{(1+z)\ln 10} \\ &= -\frac{1}{(1+z)\ln 10} \left(1 + \left[\Omega_m^{(0)}(1+z)^3 + \Omega_r^{(0)}(1+z)^4 \right. \right. \\ &\quad \left. \left. + \Omega_{DE}^{(0)} \frac{1 - \tanh\left(\Delta \log_{10}\left(\frac{1+z}{1+z_t}\right)\right)}{1 + \tanh\left(\Delta \log_{10}(1+z_t)\right)} \right]^{1/2} \right)^2. \end{aligned} \quad (38)$$

The dynamical system for the vector state $(T, \Omega_m, \Omega_r)^T$ is now given by

$$\begin{aligned} \frac{dT}{d\bar{\tau}} &= -\frac{1}{2}(T-1)T^3(2\Delta(\Omega_m + \Omega_r - 1) + \ln(10)(3\Omega_m + 4\Omega_r)) \\ &\quad + \frac{\Delta(T-1)^3T(\Omega_m + \Omega_r - 1)^2g(\Delta, z_t)}{2(\Omega_m^{(0)} + \Omega_r^{(0)} - 1)}, \end{aligned} \quad (39a)$$

$$\begin{aligned} \frac{d\Omega_m}{d\bar{\tau}} &= T^2\Omega_m(2\Delta(\Omega_m + \Omega_r - 1) + \ln(10)(3\Omega_m + 4\Omega_r - 3)) \\ &\quad + \frac{\Delta(1-T)^2\Omega_m(1-\Omega_m-\Omega_r)^2g(\Delta, z_t)}{1-\Omega_m^{(0)}-\Omega_r^{(0)}}, \end{aligned} \quad (39b)$$

$$\begin{aligned} \frac{d\Omega_r}{d\bar{\tau}} &= T^2\Omega_r(2\Delta(\Omega_m + \Omega_r - 1) + \ln(10)(3\Omega_m + 4\Omega_r - 4)) \\ &\quad + \frac{\Delta(1-T)^2\Omega_r(1-\Omega_m-\Omega_r)^2g(\Delta, z_t)}{1-\Omega_m^{(0)}-\Omega_r^{(0)}}, \end{aligned} \quad (39c)$$

with

$$g(\Delta, z_t) = \tanh(\Delta \log_{10}(z_t + 1)) + 1, \quad (40)$$

defined on the bounded phase space $\{(T, \Omega_m, \Omega_r) \in \mathbb{R}^3 : 0 \leq T \leq 1, \Omega_m + \Omega_r \leq 1, \Omega_m \geq 0, \Omega_r \geq 0\}$.

In the GEDE model, we take as the observable parameters the homogeneous constraints (which are less unbiased due to any underlying cosmology, see §3): $(\Omega_m^{(0)}, \Omega_r^{(0)}, \Omega_{DE}^{(0)}) = (0.247, 7.72 \times 10^{-5}, 0.752)$.

The stability of the equilibrium points of system (39)

are discussed in table 3³.

The system (39) admits the relevant invariant sets $T = 1$ and $T = 0$. In a similar way as for the PEDE model, the upper bounds of the parameter mean values are $z_t \sim 0.403 + 0.058 = 0.461$ (homogeneous OHD) and $\Delta \sim 0.690 + 0.624 = 1.314$ (homogeneous OHD), the dynamics is qualitatively the same as for the system (33). That is, in the invariant set $T = 1$ the equilibrium point $P_3 : (1, 0, 1)$ is a local source, $P_4 : (1, 1, 0)$ is a saddle and $P_5 : (1, 0, 0)$ is a local sink (but a saddle in the 3D phase space). On the other hand, the dynamics at the invariant set $T = 0$ is governed by an integrable 2D dynamical system, such that the line $P_7 : (0, \Omega_m, 1 - \Omega_m)$, along with the endpoints P_8 and P_9 are local attractors, whereas P_6 is the global source.

The late-time attractors on the 3D phase space are the equilibrium points $P_{1,2}$ with $T = \frac{1}{(1 \pm \tilde{\Lambda})}$, $\Omega_m = 0$, $\Omega_r = 0$, with

$$\tilde{\Lambda} \equiv \sqrt{\frac{2\Omega_{DE}^{(0)}}{g(\Delta, z_t)}}. \text{ Therefore } H_{\pm} = \pm \tilde{\Lambda}. \text{ The cosmological so-}$$

lutions corresponds to $a_{\pm}(t) = a_0 e^{\pm \tilde{\Lambda} t}$. The choice $+$, that is associated to P_1 , corresponds to an ever expanding de Sitter solution. The solution corresponding to P_2 satisfies $a \rightarrow 0$ at late times. Therefore, it is a static solution. However, this solution is not physical because the condition $T \geq 0$, requires $0 \leq \Omega_{DE}^{(0)} < \frac{g(\Delta, z_t)}{2} \sim 0.606518$, with $g(\Delta, z_t) \sim 1.213046$ where we have used the upper bounds $z_t \sim 0.461$ and $\Delta \sim 1.314$ (homogeneous OHD). This interval for $\Omega_{DE}^{(0)}$ is not supported by observations, i.e. because of the narrow bound from Planck data $\Omega_{DE}^{(0)} = 0.6889 \pm 0.0056$ by Abbott et al. (2018). With our value $\Omega_{DE}^{(0)} = 0.753^{+0.018}_{-0.017}$, the restriction has less probability to be satisfied.

There are three solutions P_3 , P_4 and P_5 dominated by radiation, dark matter and dark energy, respectively, that satisfy $T = 1$. This means that $H = 0$ at these solutions and they are saddles.

The point P_6 is the global source, it satisfies $\Omega_m = 0$, $\Omega_r = 0$, therefore, it is dominated by DE. As $T = 0$, this implies that $H \rightarrow \infty$. Because it is a source, it represents the initial stages of the cosmic evolution, dominated by DE. This means that for the model not only dark energy accounts for the recent

³ Multiplying term by term system (39) by equation (38) we obtain a system that can be integrated in terms of redshift.

Table 3. Stability of the equilibrium points of the system (39). We use the notations $g(\Delta, z_t) = \tanh\left(\frac{\Delta \ln(z_t+1)}{\ln(10)}\right) + 1$, and $\tilde{\Lambda} \equiv \sqrt{\frac{2\Omega_{\text{DE}}^{(0)}}{g(\Delta, z_t)}}$.

Label	(T, Ω_m, Ω_r)	Eigenvalues	Stability
P_1	$\left(\frac{1}{1+\tilde{\Lambda}}, 0, 0\right)$	$\left\{-\frac{4\log(10)}{(\tilde{\Lambda}+1)^2}, -\frac{3\log(10)}{(\tilde{\Lambda}+1)^2}, -\frac{2\Delta}{(\tilde{\Lambda}+1)^2}\right\}$	sink
P_2	$\left(\frac{1}{1-\tilde{\Lambda}}, 0, 0\right)$	$\left\{-\frac{4\log(10)}{(\tilde{\Lambda}-1)^2}, -\frac{3\log(10)}{(\tilde{\Lambda}-1)^2}, -\frac{2\Delta}{(\tilde{\Lambda}-1)^2}\right\}$	sink
P_3	$(1, 0, 1)$	$\{-2\ln(10), \ln(10), 2(\Delta + 2\ln(10))\}$	saddle
P_4	$(1, 1, 0)$	$\left\{-\frac{3\ln(10)}{2}, -\ln(10), 2\Delta + 3\ln(10)\right\}$	saddle
P_5	$(1, 0, 0)$	$\{\Delta, -2(\Delta + 2\ln(10)), -2\Delta - 3\ln(10)\}$	saddle
P_6	$(0, 0, 0)$	$\left\{\frac{2\Delta}{\tilde{\Lambda}^2}, \frac{2\Delta}{\tilde{\Lambda}^2}, \frac{\Delta}{\tilde{\Lambda}^2}\right\}$	source
P_7	$(0, \Omega_m, 1 - \Omega_m)$	$\{0, 0, 0\}$	nonhyperbolic
P_8	$(0, 0, 1)$	$\{0, 0, 0\}$	nonhyperbolic
P_9	$(0, 1, 0)$	$\{0, 0, 0\}$	nonhyperbolic

accelerated phase of the evolution but also for the initial expanding phase.

To analyse the non-hyperbolic points P_7 , P_8 and P_9 that satisfy $T \rightarrow 0$, we use numerical examination, where we have shown they are saddles (see Fig. 7). However, when the dynamics is restricted to the invariant set $T = 0$, it is governed by an integrable 2D dynamical system, such that the line $P_7 : (0, \Omega_m, 1 - \Omega_m)$, along with the endpoints P_8 and P_9 are local attractors, whereas P_6 is the global source. The dynamics is exactly the same as presented in Fig. 6 after τ is re-scaled by the factor $\frac{1 - \Omega_m^{(0)} - \Omega_r^{(0)}}{\Delta g(\Delta, z_t)} > 0$.

Figure 7 shows the dynamics of the systems (33) for the PEDE model with $(\Omega_m^{(0)}, \Omega_r^{(0)}) = (0.252, 7.62 \times 10^{-5})$ and (39) for the GEDE model with $(\Omega_m^{(0)}, \Omega_r^{(0)}) = (0.247, 7.72 \times 10^{-5})$. The blue lines correspond to orbits with initial condition $(T(0), \Omega_m(0), \Omega_r(0)) = (0.5, 0.252, 7.62 \times 10^{-5})$ and $(0.5, 0.247, 7.72 \times 10^{-5})$, for PEDE and GEDE respectively, which represent the current universe. All orbits are attracted by the point (marked with a star) $P_1 : (T, \Omega_m, \Omega_r) = (0.449833, 0., 0.)$ (PEDE) and $P_1 : (T, \Omega_m, \Omega_r) = (0.472999, 0., 0.)$ (GEDE). We have evaluated $g(\Delta, z_t) \sim 1.213046$ using the upper bounds of $z_t \sim 0.461$ and $\Delta \sim 1.314$ (homogeneous OHD).

The top panel of Figure 8 shows the numerical solution for the system (33) (PEDE) and (39) (GEDE) using the initial conditions at current epoch. For this particular solution, at early epochs, the universe is dominated by radiation (equilibrium point P_8), later on, the matter becomes equal to radiation, then it begins to dominate (equilibrium point P_9). At late times, the emergent DE dominates the Universe dynamics in a de Sitter phase (equilibrium point P_1). The aforementioned radiation dominated solution P_8 and the matter dominated solution P_4 do have $T = 0$. This means that $H \rightarrow \infty$ at these solutions, as expected ($H \sim \frac{1}{2t}$ for the usual radiation dominated solution and $H \sim \frac{2}{3t}$ for the usual matter dominated solution). In the bottom panel of the same figure, it is shown the difference between the dynamical variables for the GEDE and PEDE models.

5 CONCLUSIONS

We investigated the phenomenological models recently proposed by Li & Shafieloo (2019, 2020) for which the dark en-

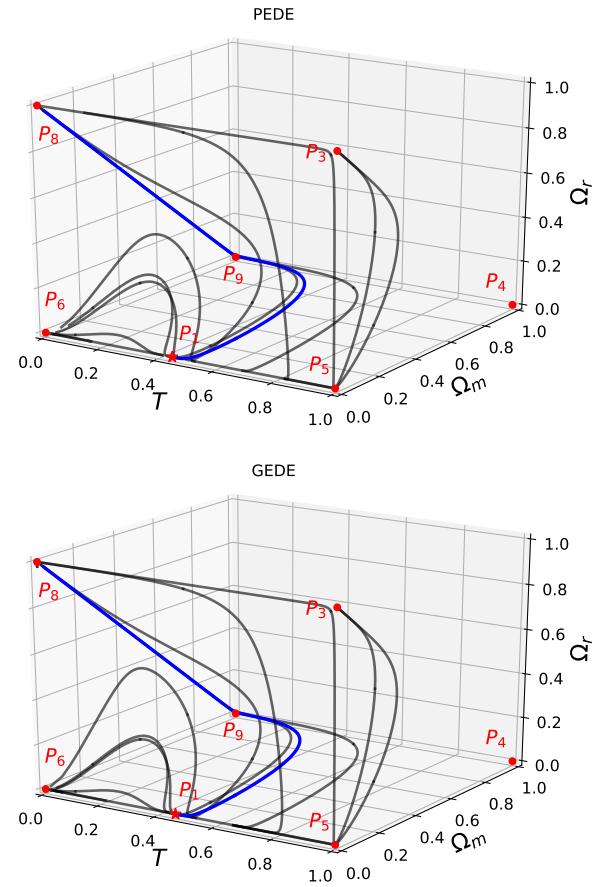


Figure 7. Dynamics of the systems (33) for the PEDE model with $(\Omega_m^{(0)}, \Omega_r^{(0)}) = (0.252, 7.62 \times 10^{-5})$ (top panel) and (39) for the GEDE model with $(\Omega_m^{(0)}, \Omega_r^{(0)}) = (0.247, 7.72 \times 10^{-5})$ (bottom panel). The blue lines correspond to the orbit with initial condition $(T(0), \Omega_m(0), \Omega_r(0)) = (0.5, 0.252, 7.62 \times 10^{-5})$ and $(0.5, 0.247, 7.72 \times 10^{-5})$, for PEDE and GEDE respectively, which represents the current universe. We see that all orbits are attracted by the point (marked with a star) $P_1 : (T, \Omega_m, \Omega_r) = (0.449833, 0., 0.)$ (PEDE) and $P_1 : (T, \Omega_m, \Omega_r) = (0.472999, 0., 0.)$ (GEDE).

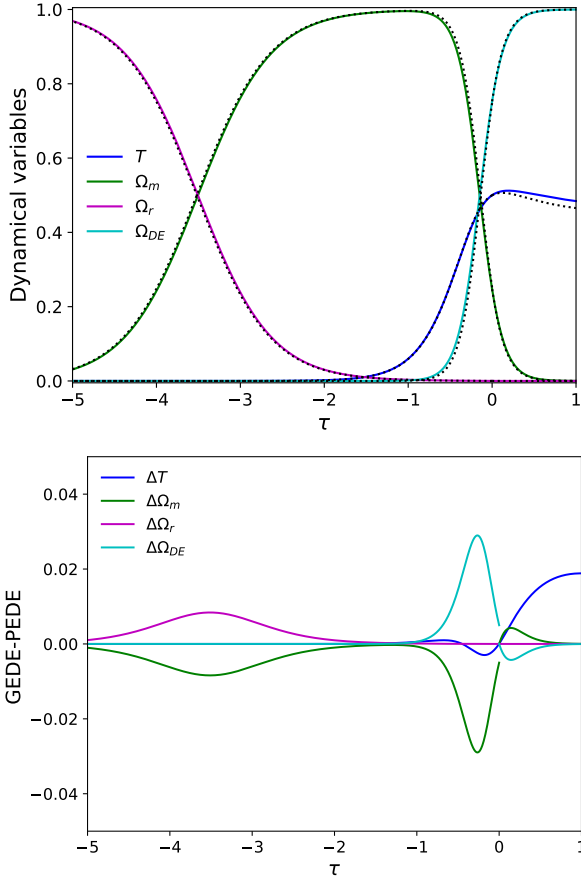


Figure 8. Top panel. Evolution of the dynamical variables ($T, \Omega_m, \Omega_r, \Omega_{DE}$) over τ for the GEDE model. In dotted-black lines are the corresponding variables for the PEDE model. Bottom panel. $\Delta\Omega_i = \Omega_i^{GEDE} - \Omega_i^{PEDE}$ for $i = m, r, DE$ and $\Delta T = T^{GEDE} - T^{PEDE}$.

ergy is negligible at very early times of the Universe, dubbed PEDE and GEDE models. The main characteristic of these models is that they emerge at late times sourcing the accelerated expansion of the Universe through $\Omega_{DE}(z) \propto \tanh(z)$. While in PEDE model there is no extra degree of freedom as the standard model, the GEDE model introduces one free parameter (Δ) which plays an important role to recover the Λ CDM and PEDE dynamics when $\Delta = 0$ and $\Delta = 1$, respectively.

We put observational constraints for the PEDE and GEDE models through the most recent observational Hubble data samples: one including non-homogeneous OHD points from BAO and other sample where they are homogeneous. Our analysis was performed with flat and Gaussian priors on the dimensionless Hubble parameter at the today h . Our constraints for the PEDE model are consistent with those obtained by Li & Shafieloo (2019). Nevertheless, our Δ limits (e.g. $0.69^{+0.624}_{-0.457}$) are consistent with PEDE model but in tension at 1σ with $\Delta = 1.13 \pm 0.28$ obtained by Li & Shafieloo (2020) from Planck and H_0 (R19) measurements. Considering the uncertainties on Δ , there is no strong support of GEDE over the Λ model when OHD (low redshift)

are employed. In addition, we also reconstructed the cosmic evolution for the deceleration and jerk parameters in the PEDE and GEDE scenarios. For both models, the deceleration parameter undergoes a phase transition from a decelerated expansion to an accelerated one (at $z \sim 0.78, 0.8$). By construction PEDE and GEDE are dynamical dark energy models, hence the jerk parameter deviates from one. Furthermore, our values for the deceleration-acceleration transition redshift and current values of the cosmographic parameters q_0 and j_0 are in agreement with those reported in the literature (García-Aspeitia et al. 2018c; Haridasu et al. 2018; Hernández-Almada 2019; Hernández-Almada et al. 2020). Regarding our stability analysis, we reconstructed the evolution of the dynamical variables Ω_m, Ω_r , and Ω_{DE} for PEDE and GEDE models using the homogeneous constraints since they are less unbiased due to any underlying cosmology (see §3). We obtain that they have a very similar dynamics (Fig. 8). We see that the Universe evolves to a de Sitter solution, corresponding to the equilibrium point P_1 with $a_+(t) = a_0 e^{\hat{\Lambda}t}$, (see §4) from a matter dominated phase, preceded by a radiation dominated epoch. However, the main difference with the evolution of the Λ CDM model is that the global source (equilibrium point P_6) is dominated by DE. This means that for the model not only dark energy accounts for the recent accelerated phase of the evolution but also the initial stages are driven by a DE dominated accelerated expanding phase. This feature of PEDE/GEDE models is not mentioned by Li & Shafieloo (2019, 2020). Furthermore, there is a possibility to have an attractor in P_2 , with $a_-(t) = a_0 e^{-\hat{\Lambda}t}$, which is not an expanding solution for $H_0 > 0$ at late times. However, this solution is not supported by data (Abbott et al. 2018) because the condition $T \geq 0$ requires $0 \leq \Omega_{DE}^{(0)} < \frac{1}{2}$ (PEDE, homogeneous OHD), or $0 \leq \Omega_{DE}^{(0)} < \frac{g(\Delta, z_t)}{2} \sim 0.606518$ (GEDE, homogeneous OHD). In addition, our constraints (homogeneous OHD) are $\Omega_{DE}^{(0)} = 0.748^{+0.016}_{-0.015}$, $\Omega_r^{(0)} = (7.63^{+0.24}_{+0.23}) \times 10^{-5}$ for PEDE and $\Omega_{DE}^{(0)} = 0.753^{+0.018}_{-0.017}$, $\Omega_r^{(0)} = (7.72^{+0.26}_{+0.25}) \times 10^{-5}$ for GEDE, which makes the condition of existence for P_2 hardest to be satisfied.

On the other hand, many emergent DE models as those studied by García-Aspeitia et al. (2019a) based on unimodular gravity, predict a birth of DE in the reionization epoch at $z \sim 17$, where an excess of photons has been detected by EDGES (Bowman et al. 2018) that could imply new physics beyond the standard scenario. In this vein, the PEDE (GEDE) model could also emerge at the same epoch, being in agreement with the unimodular gravity. At $z \sim 17$, the PEDE density is $\rho_{DE} \sim 10\% \rho_c^{(0)}$ (i.e. $\Omega_{DE} \sim 0.1$). Finally, the early accelerated phase, a possible connection to the reionization epoch together with other observational constraints, could be transcendental for PEDE and GEDE models and they should be further investigated.

ACKNOWLEDGMENTS

G.L. was funded by CONICYT through FONDECYT Iniciación grant no. 11180126 and by Vicerrectoría de Investigación y Desarrollo Tecnológico at Universidad Católica del Norte., J.M. acknowledges the support from CONICYT project Basal AFB-170002, M.A.G.-A. ac-

knowledges support from SNI-México, CONACyT research fellow, COZCyT and Instituto Avanzado de Cosmología (IAC) collaborations. V.M. acknowledges the support of Centro de Astrofísica de Valparaíso (CAV). J.M., M.A.G.-A and V.M. acknowledge CONICYT REDES (190147).

NOTE ADDED

While this work was being typed, we became aware of a complementary study of PEDE model, developed by Liu & Miao (2020), that appeared in the arXiv repository. Liu & Miao (2020), used CMB data from Planck 2018, BAO measurements and SNIa data, to obtain the bounds on total neutrino masses with the approximation of degenerate neutrino masses, in some Dark Energy settings, in particular in PEDE models.

REFERENCES

- Abbott T. M. C., et al., 2018, *Monthly Notices of the Royal Astronomical Society*, 480, 3879
- Aghanim N., et al., 2018
- Amante M. H., Magaña J., Motta V., García-Aspeitia M. A., Verdugo T., 2019, arXiv e-prints, [p. arXiv:1906.04107](https://arxiv.org/abs/1906.04107)
- Armendariz-Picon C., Mukhanov V. F., Steinhardt P. J., 2000, *Phys. Rev. Lett.*, 85, 4438
- Armendariz-Picon C., Mukhanov V. F., Steinhardt P. J., 2001, *Phys. Rev.*, D63, 103510
- Bamba K., Capozziello S., Nojiri S., Odintsov S. D., 2012, *Astro-phys. Space Sci.*, 342, 155
- Barboza Jr. E. M., Alcaniz J. S., 2008, *Phys. Lett.*, B666, 415
- Basilakos S., Leon G., Papagiannopoulos G., Saridakis E. N., 2019, *Phys. Rev.*, D100, 043524
- Bolotin Y. L., Kostenko A., Lemets O. A., Yerokhin D. A., 2015, *International Journal of Modern Physics D*, 24, 1530007
- Bowman J. D., Rogers A. E. E., Monsalve R. A., Mozdzen T. J., Mahesh N., 2018, *Nature*, 555, 67
- Caldera-Cabral G., Maartens R., Ureña López L. A., 2009, *Phys. Rev. D*, 79, 063518
- Caldwell R. R., 2002, *Phys. Lett.*, B545, 23
- Caldwell R. R., Dave R., Steinhardt P. J., 1998, *Phys. Rev. Lett.*, 80, 1582
- Capozziello S., Cardone V. F., Elizalde E., Nojiri S., Odintsov S. D., 2006a, *Phys. Rev.*, D73, 043512
- Capozziello S., Nojiri S., Odintsov S. D., 2006b, *Phys. Lett.*, B632, 597
- Chen X.-m., Gong Y.-g., Saridakis E. N., 2009, *JCAP*, 0904, 001
- Chevallier M., Polarski D., 2001, *Int. J. Mod. Phys.*, D10, 213
- Chiba T., Nakamura T., 1998, *Progress of Theoretical Physics*, 100, 1077
- Chiba T., Okabe T., Yamaguchi M., 2000, *Phys. Rev.*, D62, 023511
- Cid A., Leon G., Leyva Y., 2016, *JCAP*, 1602, 027
- Cid A., Izaurieta F., Leon G., Medina P., Narbona D., 2018, *JCAP*, 1804, 041
- Coley A. A., 2003, *Dynamical systems and cosmology*. Vol. 291, Kluwer, Dordrecht, Netherlands, [doi:10.1007/978-94-017-0327-7](https://doi.org/10.1007/978-94-017-0327-7)
- Coley A., Leon G., 2019, *Gen. Rel. Grav.*, 51, 115
- Copeland E. J., Liddle A. R., Wands D., 1998, *Phys. Rev.*, D57, 4686
- Copeland E. J., Sami M., Tsujikawa S., 2006, *Int. J. Mod. Phys.*, D15, 1753
- Cotsakis S., Kittou G., 2013, *Phys. Rev.*, D88, 083514
- Cruz N., Hernández-Almada A., Cornejo-Pérez O., 2019, *Phys. Rev.*, D100, 083524
- De Arcia R., Gonzalez T., Leon G., Nucamendi U., Quiros I., 2016, *Class. Quant. Grav.*, 33, 125036
- De Arcia R., Gonzalez T., Horta-Rangel F. A., Leon G., Nucamendi U., Quiros I., 2018, *Class. Quant. Grav.*, 35, 145001
- Dhawan S., Brout D., Scolnic D., Goobar A., Riess A. G., Miranda V., 2020, Cosmological model insensitivity of local H_0 from the Cepheid distance ladder ([arXiv:2001.09260](https://arxiv.org/abs/2001.09260))
- Di Valentino E., Melchiorri A., Mena O., Vagnozzi S., 2019
- Dimakis N., Giacomini A., Jamal S., Leon G., Paliathanasis A., 2017, *Phys. Rev.*, D95, 064031
- Fadragas C. R., Leon G., 2014, *Class. Quant. Grav.*, 31, 195011
- Fadragas C. R., Leon G., Saridakis E. N., 2014, *Class. Quant. Grav.*, 31, 075018
- Ferreira P. G., Joyce M., 1997, *Phys. Rev. Lett.*, 79, 4740
- Foreman-Mackey D., Hogg D. W., Lang D., Goodman J., 2013, *pasp*, 125, 306
- García-Aspeitia M. A., Magaña J., Hernández-Almada A., Motta V., 2018a, *International Journal of Modern Physics D*, 27, 1850006
- García-Aspeitia M. A., Hernández-Almada A., Magaña J., Amante M. H., Motta V., Martínez-Robles C., 2018b, *Phys. Rev. D*, 97, 101301
- García-Aspeitia M. A., Hernández-Almada A., Magaña J., Amante M. H., Motta V., Martínez-Robles C., 2018c, *Phys. Rev.*, D97, 101301
- García-Aspeitia M. A., Hernández-Almada A., Magaña J., Motta V., 2019a
- García-Aspeitia M. A., Hernández-Almada A., Magaña J., Motta V., 2019b, arXiv e-prints, [p. arXiv:1912.07500](https://arxiv.org/abs/1912.07500)
- García-Aspeitia M. A., Martínez-Robles C., Hernández-Almada A., Magaña J., Motta V., 2019c, *Phys. Rev. D*, 99, 123525
- Giacomini A., Jamal S., Leon G., Paliathanasis A., Saavedra J., 2017, *Phys. Rev.*, D95, 124060
- Giacomini A., Leon G., Paliathanasis A., Pan S., 2020
- Giambo R., Miritzis J., 2010, *Class. Quant. Grav.*, 27, 095003
- Guo Z.-K., Piao Y.-S., Zhang X.-M., Zhang Y.-Z., 2005, *Phys. Lett.*, B608, 177
- Haridasu B. S., Luković V. V., Moresco M., Vittorio N., 2018, *Journal of Cosmology and Astroparticle Physics*, 2018, 015
- Hernández-Almada A., 2019, *The European Physical Journal C*, 79, 751
- Hernández-Almada A., Magaña J., García-Aspeitia M. A., Motta V., 2019, *European Physical Journal C*, 79, 12
- Hernández-Almada A., García-Aspeitia M. A., Magaña J., Motta V., 2020, Stability analysis and constraints on interacting viscous cosmology ([arXiv:2001.08667](https://arxiv.org/abs/2001.08667))
- Holsclaw R., Alam U., Sansó B., Lee H., Heitmann K., Habib S., Higdon D., 2010, *Phys. Rev. D*, 82, 103502
- Jassal H. K., Bagla J. S., Padmanabhan T., 2005, *Mon. Not. Roy. Astron. Soc.*, 356, L11
- Jesus J. F., Holanda R. F. L., Pereira S. H., 2018, *J. Cosmology Astropart. Phys.*, 2018, 073
- Jimenez R., Loeb A., 2002, *ApJ*, 573, 37
- Karpathopoulos L., Basilakos S., Leon G., Paliathanasis A., Tsamparlis M., 2018, *Gen. Rel. Grav.*, 50, 79
- Kofinas G., Leon G., Saridakis E. N., 2014, *Class. Quant. Grav.*, 31, 175011
- Komatsu E., et. al. 2011, *The Astrophysical Journal Supplement Series*, 192, 18
- Latta J., Leon G., Paliathanasis A., 2016, *JCAP*, 1611, 051
- Lazkoz R., Leon G., 2006, *Phys. Lett.*, B638, 303
- Lazkoz R., Leon G., Quiros I., 2007, *Phys. Lett.*, B649, 103
- Leon G., 2009, *Class. Quant. Grav.*, 26, 035008
- Leon G., Paliathanasis A., 2019, *Eur. Phys. J.*, C79, 746
- Leon G., Saridakis E. N., 2009, *JCAP*, 0911, 006
- Leon G., Saridakis E. N., 2013, *JCAP*, 1303, 025

- Leon G., Saridakis E. N., 2015, *JCAP*, 1504, 031
- Leon G., Silva F. O. F., 2019
- Leon G., Saavedra J., Saridakis E. N., 2013, *Class. Quant. Grav.*, 30, 135001
- Leon G., Paliathanasis A., Morales-Martínez J. L., 2018, *Eur. Phys. J.*, C78, 753
- Leon G., Coley A., Paliathanasis A., 2020, *Annals Phys.*, 412, 168002
- León G., Paliathanasis A., Velazquez L. A., 2018
- Li X., Shafieloo A., 2019, *ApJ*, 883, L3
- Li X., Shafieloo A., 2020, arXiv e-prints, p. [arXiv:2001.05103](https://arxiv.org/abs/2001.05103)
- Li M., Li X.-D., Wang S., Wang Y., 2011, *Commun. Theor. Phys.*, 56, 525
- Linder E. V., 2003, *Phys. Rev. Lett.*, 90, 091301
- Liu Z., Miao H., 2020
- Magaña J., Motta V., Cardenas V. H., Foex G., 2017, *Mon. Not. Roy. Astron. Soc.*, 469, 47
- Magaña J., Amante M. H., García-Aspeitia M. A., Motta V., 2018, *Monthly Notices of the Royal Astronomical Society*, 476, 1036
- Moresco M., et al., 2012, *J. Cosmology Astropart. Phys.*, 2012, 006
- Mortonson M., Hu W., Huterer D., 2009, *Physical Review D*, 80
- Övgün A., Leon G., Magaña J., Jusufi K., 2018, *European Physical Journal C*, 78, 462
- Perko L., 2000, *Differential Equations and Dynamical Systems*, Third Edition. Springer
- Perlmutter S., Aldering G., Goldhaber G., Knop R. A., Nugent P., others Project T. S. C., 1999, *The Astrophysical Journal*, 517, 565
- Pulgar G., Saavedra J., Leon G., Leyva Y., 2015, *JCAP*, 1505, 046
- Riess A. G., Filippenko A. V., Challis P., Clocchiatti A., Diercks A., et al., 1998, *The Astronomical Journal*, 116, 1009
- Riess A. G., Casertano S., Yuan W., Macri L. M., Scolnic D., 2019, *The Astrophysical Journal*, 876, 85
- Román-Garza J., Verdugo T., Magaña J., Motta V., 2019, *European Physical Journal C*, 79, 890
- Sendra I., Lazkoz R., 2012, *MNRAS*, 422, 776
- Sola Peracaula J., Gomez-Valent A., de Cruz Pérez J., 2019, *Phys. Dark Univ.*, 25, 100311
- Tsujikawa S., 2011, *Dark Energy: Investigation and Modeling*. Springer Netherlands, Dordrecht, pp 331–402, doi:10.1007/978-90-481-8685-3_8, https://doi.org/10.1007/978-90-481-8685-3_8
- Tsujikawa S., 2013, *Class. Quant. Grav.*, 30, 214003
- Verde L., Treu T., Riess A. G., 2019, in *Nature Astronomy* 2019. ([arXiv:1907.10625](https://arxiv.org/abs/1907.10625)), doi:10.1038/s41550-019-0902-0
- Wainwright J., Ellis G. F. R., 1997, *Dynamical Systems in Cosmology*. Cambridge University Press
- Weinberg S., 1989, *Reviews of Modern Physics*, 61
- Wetterich C., 1988, *Nuclear Physics B*, 302, 668
- Xu C., Saridakis E. N., Leon G., 2012, *JCAP*, 1207, 005
- Zel’dovich Y. B., 1968, *Soviet Physics Uspekhi*, 11, 381
- Zhao G.-B., Raveri M., et. al. 2017, *Nature Astronomy*, 1, 627–632